Flux Crystal Growth of a New $BaTa_2O_6$ Polymorph, and of the Novel Tantalum Oxyfluoride Salt Inclusion Phase $[Ba_3F]Ta_4O_{12}F$: Flux Dependent Phase Formation

Ceren Kutahyali Aslani, Vladislav V. Klepov, and Hans-Conrad zur Loye[*]

Department of Chemistry and Biochemistry, University of South Carolina, Columbia, SC 29208

Abstract:

A new hexagonal polymorph of $BaTa_2O_6$ and a novel salt inclusion phase, $[Ba_3F]Ta_4O_{12}F$, were obtained *via* high temperature flux crystal growth using mixed alkali chloride / alkali fluoride fluxes. $BaTa_2O_6$ and $[Ba_3F]Ta_4O_{12}F$ crystallize in the hexagonal and tetragonal space groups *P*6/*mmm* and $P4_2/mnm$, respectively. The structure of $BaTa_2O_6$ consists of TaO_6 octahedra that edge-share *via* equatorial O(2) to form Ta_2O_{10} dimers that further connect to form a 3D structure containing channels in which the barium cations are located. The morphology of this structure is substantially different from those of the three previously reported polymorphs of $BaTa_2O_6$. The structure of the salt inclusion phase, $[Ba_3F]Ta_4O_{12}F$, consists of slightly zig-zagging chains of trans corner-sharing (*via* O(3) and O(4)) TaO_6 octahedra that corner-share their equatorial O(1) and O(5) oxygens with TaO_5F octahedra to create the framework for the Ba_3F salt inclusion. The stability of $BaTa_2O_6$ polymorphs was assessed using DFT calculations. The new hexagonal polymorph ($\Delta_f H_{0\,K}$ of -2825.11 kJ/mol) has a higher energy than the other three known phases and is 49.17 kJ/mol higher than the next most stable polymorph.

Introduction

Barium tantalum oxides have been of interest for a number of applications, including photocatalysis [1], dielectric materials [2,3], and as photoluminescent hosts [4]. For that reason, several different synthetic approaches have been used to prepare nanoparticles, polycrystalline powders and single crystals of diverse Ba-Ta-O compositions. One outcome of this interest in barium tantalates has been an extensive investigation of the BaO-Ta_2O_5 phase diagram, which was found to contain several complex barium titanate compositions including $Ba_6Ta_2O_{11}$ ($6BaO+Ta_2O_5$) [5], $Ba_4Ta_2O_9$ ($4BaO+Ta_2O_5$) [6], $Ba_5Ta_4O_{15}$ ($5BaO+2Ta_2O_5$) [7,8], $BaTa_4O_{11}$ ($BaO+2Ta_2O_5$) [9] and $BaTa_2O_6$ ($BaO+Ta_2O_5$) [1, 10-12]. The latter has the simplest composition, consisting of one BaO and one Ta_2O_5 unit. Until now, three polymorphs of $BaTa_2O_6$ had been described in the literature, a hexagonal phase, a tetragonal phase with the potassium tungsten bronze structure, and an orthorhombic phase. Now, as described herein, a second hexagonal phase has been identified and obtained *via* high temperature flux crystal growth.

The first reports of $BaTa_2O_6$ date back to the work of Ismailzade who in the late 50s reported on a tetragonal [13] $BaTa_2O_6$ phase, (a = 17.800, c = 7.84 Å) and an orthorhombic [14] phase (a = 17.645, b = 17.866, and c = 7.791 Å), and the work of Galasso *et al*. [12] who reported on a tetragonal $BaTa_2O_6$ phase (a = 12.60, c = 3.95 Å). Layden [10] in the sixties published on the presence of three polymorphs with orthorhombic (a = 12.33, b = 10.26, c = 7.67 Å), tetragonal (a = 12.52, c = 3.956 Å) and hexagonal (a = 21.14, c = 3.917 Å) symmetry unit cells. The structure of the hexagonal phase, confirmed by a single crystal structure report by Mumme *et al*. [1], is considered the most accurate description of the hexagonal phase to date. In their publication the authors suggested that the hexagonal form is the high temperature (above 1300 °C) stable form. Work by Galasso *et al*. [12] suggests that the orthorhombic form is the low temperature form and, also, that the hexagonal form is the high temperature form.

	$BaTa_2O_6$-H	$BaTa_2O_6$-T	$BaTa_2O_6$-O	$BaTa_2O_6$-H-new
a, Å	21.116(1)	12.55819(8)	17.645	10.6652(2)
b, Å			17.866	
c, Å	3.9157(2)	3.94503(3)	7.791	3.9597(1)
	*P*6/*mmm*	*P*4/*mbm*	orthorhombic	*P*6/*mmm*
	Mumme *et al*. [1]	Kim *et al*. [15]	Ismailzade [14]	This work

The work by Mumme *et al*. [1] reports the crystal growth of hexagonal bronze type $BaTa_2O_6$ using a vanadate flux. Crystals were grown using a pre-reacted $BaO:Ta_2O_5$ powder that was dissolved in a $BaO:V_2O_5$ melt at 1400 °C for 2 h in a platinum crucible. Slow cooling to 600 °C resulted in crystals of different shapes that corresponded to all three known polymorphs. Using a CsCl/CsF flux we obtained a new hexagonal phase of $BaTa_2O_6$ described herein. Interestingly, using a RbCl/RbF flux, under otherwise identical reaction conditions, the salt inclusion material (SIM) $[Ba_3F]Ta_4O_{12}F$ was obtained rather than $BaTa_2O_6$. The structure of $[Ba_3F]Ta_4O_{12}F$ is described herein as well. This phase is isostructural with $[Pb_3F]M_4O_{12}F$ (M = Nb, Ta) reported by Savborg and Lundberg [16] which crystallize tetragonal space group $P4_2/mnm$.

It is known that the use of different fluxes under otherwise identical reaction conditions can result in dramatically different products and, furthermore, that it is difficult to predict ahead of time whether or not a flux will be passive and not end up incorporated in the product, or reactive, which results in some flux components becoming incorporated into the product phase [17,18]. Fluoride containing melts are known to be reactive and often result in oxyfluoride products or salt inclusion phases. In fact, a large number of SIMs have been synthesized using CsCl/CsF melts [19-21]. The melting point of the flux versus the reaction temperature, which determines the liquid range of the crystallization process is thought to contribute, in addition to chemical differences, to the determination of the product that crystallizes. Herein we discuss the synthesis of $BaTa_2O_6$ and $[Ba_3F]Ta_4O_{12}F$ and using DFT calculations, explore the relative stability of the different $BaTa_2O_6$ polymorphs.

Experimental

Reagents

$BaCO_3$ (Alfa Aesar, 99.95%), Ta_2O_5 (Alfa Aesar, 99%), RbCl (Alfa Aesar, 99.8%), RbF (99.1%, Alfa Aesar), CsCl (Ultra-pure, VWR) and CsF (Alfa Aesar, 99.9%) were used as received without any further modification for the synthesis of both title compounds.

Flux Growth

Crystal growth of $BaTa_2O_6$: $BaCO_3$ (0.100 g) and Ta_2O_5 (0.448 g), a molar ratio of 2:1, were mixed with 1 g of a 50:50 mixture by weight of CsCl/CsF. The reagents were placed into a 7.5 cm tall by 1.2 cm diameter silver tube that was welded shut at one end and crimped shut at the other and heated to 800 °C in 1 h, held at that temperature for 20 h and then slow cooled at

20°C/h rate to 400 °C. At that point the furnace was shut off and the sample cooled to room temperature. The crystals were isolated from the flux by dissolving the flux in water, aided by sonication.

Crystal growth of $[Ba_3F]Ta_4O_{12}F$: $BaCO_3$ (0.100 g) and Ta_2O_5 (0.448 g), a molar ratio of 2:1, were mixed with 1 g of a 50:50 mixture by weight of RbCl/RbF. The reagents were placed into a 7.5 cm tall by 1.2 cm diameter silver tube that was welded shut at one end and crimped shut at the other and heated to 800 °C in 1 h, held at that temperature for 20 h and then slow cooled at 20°C/h rate to 400 °C. At that point the furnace was shut off and the sample cooled to room temperature. The crystals were isolated from the flux by dissolving the flux in water, aided by sonication.

Figure 1a shows the silver tube that used in the experiments. An optical image of single crystals of the $BaTa_2O_6$ and $[Ba_3F]Ta_4O_{12}F$ are provided in Figure 1b.

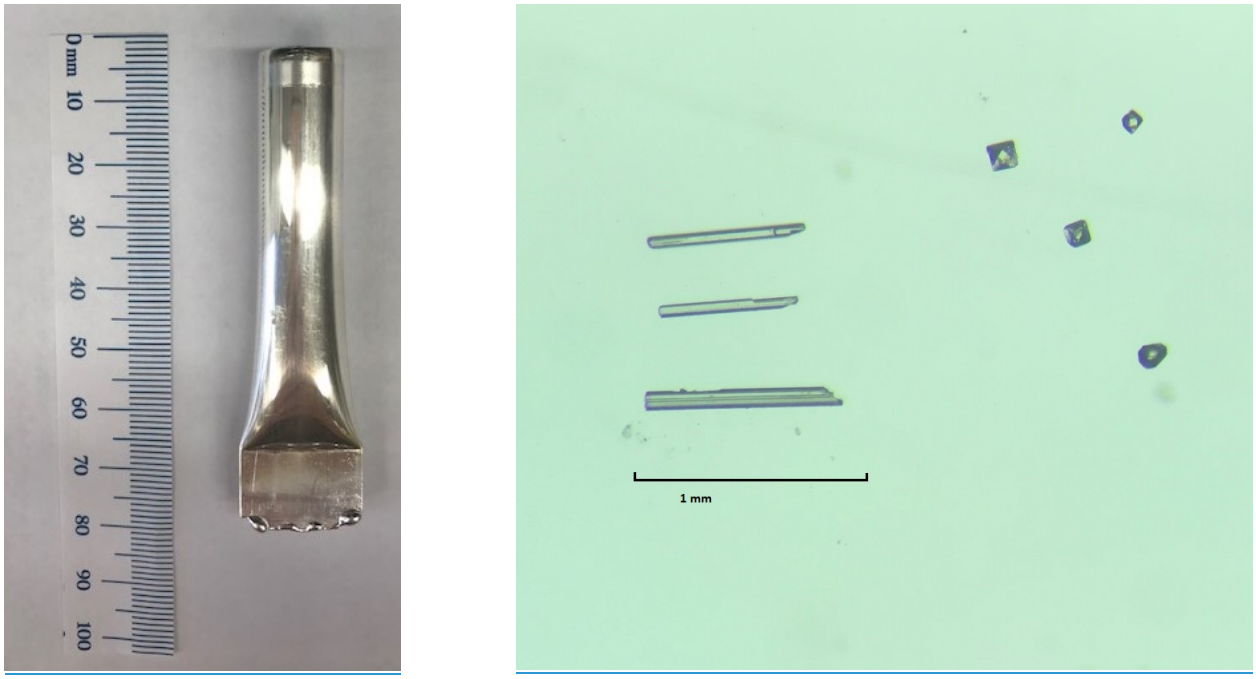

(a) (b)

Figure 1. (a) Silver tube (b) Optical images of single crystals of $BaTa_2O_6$ (left) and $[Ba_3F]Ta_4O_{12}F$ (right).

PXRD. Powder X-ray diffraction (PXRD) data were collected on all compounds using a Bruker D2 Phaser equipped with an LYNXEYE silicon strip detector and a Cu Kα source to identify and to evaluate the phase purity of the samples.

SXRD. The structure of each compound was determined by single crystal X-ray diffraction data collected on a Bruker D8 QUEST single crystal X-ray diffractometer equipped with an Incoatec IμS 3.0 Mo Kα microfocus source and a PHOTON II area detector. The data were reduced and corrected for sample absorption using the SAINT+ and SADABS programs within the APEX 3 software [22,23]. The SHELX software suite was used within the Olex 2 GUI to solve and refine the structures [24]. The intrinsic phasing solution method, SHELXT, and the least squares refinement method, SHELXL were used [25]. The crystallographic data and results of the diffraction experiments are summarized in Table 1. $BaTa_2O_6$ was initially refined anisotropically, which resulted in a reasonable thermal ellipsoid for all except one atom, O(1). The presence of a large positive electron density peak next to O(1) atomic position and its elongated thermal ellipsoid indicated disorder of this atom. After trying several different models for the disordered atom, the best model was picked, in which O(1) position with a C_{2v} site-symmetry and a 0.26 occupancy is surrounded by two satellite O(4) sites with 0.37 site occupancy that are related to each other by a mirror plane. Anisotropic refinement of O(1) and O(4) sites results in negative thermal parameters, thus both of them were refined isotropically, yielding a good R_1 value of 1.18% and no large residual electron density peaks. $[Ba_3F]Ta_4O_{12}F$ contains both O and F atoms, which are difficult to distinguish, especially in the presence of heavy elements, such as Ba and Ta. One anion site that is surrounded by four Ba atoms was identified as a fluorine site that forms a salt-inclusion. Locating the second fluorine atom, which was required to charge balance the formula, was more ambiguous. Since fluorine atoms tend not to play the role of a bridging atom, the only terminal oxygen site O(2) was refined as half oxygen/half fluorine site, resulting in the $[Ba_3F]Ta_4O_{12}F$ formula.

Table 1. Crystallographic data for $BaTa_2O_6$ and $[Ba_3F]Ta_4O_{12}F$

Formula	$BaTa_2O_6$	$[Ba_3F]Ta_4O_{12}F$
Formula weight	595.24	1365.82
Temperature/K	301.45	302.24
Crystal system	hexagonal	tetragonal
Space group	*P*6/*mmm*	$P4_2/mnm$

a/Å	10.6652(2)	12.7615(3)
b/Å	10.6652(2)	12.7615(3)
c/Å	3.95970(10)	7.5013(2)
α/°	90	90
β/°	90	90
γ/°	120	90
Volume/$Å^3$	390.059(18)	1221.63(7)
Z	3	4
$\rho_{calc}g/cm^3$	7.602	7.426
μ/mm^{-1}	49.412	45.265
F(000)	750	2296
Crystal size/mm^3	0.04 × 0.02 × 0.02	0.06 × 0.03 × 0.02
Radiation	MoKα (λ = 0.71073)	
2θ range for data collection/°	7.642 to 57.838	6.3 to 54.994
Index ranges	$-14 \le h \le 14$, $-14 \le k \le 14$, $-5 \le l \le 5$	$-16 \le h \le 16$, $-16 \le k \le 16$, $-9 \le l \le 9$
Reflections collected	19284	47229
Independent reflections	243 [R_{int} = 0.0319, R_{sigma} = 0.0064]	804 [R_{int} = 0.0400, R_{sigma} = 0.0083]
Data/restraints/parameters	243/0/23	804/0/64
Goodness-of-fit on F^2	1.194	1.18
Final R indexes [I>=2σ (I)]	R_1 = 0.0118, wR_2 = 0.0299	R_1 = 0.0137, wR_2 = 0.0330
Largest diff. peak/hole / e $Å^{-3}$	1.02/-0.92	1.68/-1.20

First-Principles Calculations. We performed first-principles calculations in the form of density functional theory (DFT), using the Vienna Ab-initio Package (VASP) planewave code [26,27] generalized gradient approximation of Perdew, Burke and Ernzerhof (PBE) [28] and projector augmented wave (PAW) method [29,30]. As there is no single crystal structure reported for the orthorhombic $BaTa_2O_6$, but it is known to be isostructural with $BaNb_2O_6$, the latter structure was used for geometry optimization [12]. Spin-polarized calculations were performed, with 520 eV cut-off energy for the plane wave basis set, 10^{-6} eV energy convergence criteria and 3×3×13, 4×4×13, 6×4×5, and 5×5×13 *k*-point mesh for $BaTa_2O_6$-H, $BaTa_2O_6$-T, $BaTa_2O_6$-O, and $BaTa_2O_6$-H-new, respectively. The ground state geometries at 0 K were optimized by relaxing the cell volume, atomic positions, and cell symmetry until the maximum force on each atom is less than 0.001 eV/Å. The enthalpies of formation of each phase were calculated using the OQMD formation energies of the constituent elements [31].

Results and discussion

Single crystals of $BaTa_2O_6$ and $[Ba_3F]Ta_4O_{12}F$ were isolated from mixed alkali metal chloride fluoride fluxes. Mixed chloride fluoride fluxes are well known to readily crystallize complex oxides and, at times, oxyfluorides [32,33]. The crystallization of pure oxide phases can occur with or without the incorporation of any flux elements, as is observed for the crystallization of $BaTa_2O_6$. On the other hand, elements of the flux are known to end up in the crystalline products when the flux is "reactive", and this was the case in the crystallization of $[Ba_3F]Ta_4O_{12}F$. The crystals were isolated in low yield (< 10%) and their structures determined by single crystal X-ray diffraction. According to PXRD results, in addition to $BaTa_2O_6$, there is an unidentified impurity, the crystals of which are of poor quality, preventing their structure determination by single crystal X-ray diffraction. In the reactions that yielded $[Ba_3F]Ta_4O_{12}F$, BaF_2 and $RbTa_2O_5F$ were also found to have formed. All reactions are reproducible and while increasing the flux amount to 2 g for a 50:50 mixture does not affect the formation of $BaTa_2O_6$, it does eliminate the formation of $[Ba_3F]Ta_4O_{12}F$.

$BaTa_2O_6$ crystallizes in the hexagonal space group *P*6/*mmm* and $[Ba_3F]Ta_4O_{12}F$ crystallizes in the tetragonal space group $P4_2/mnm$. Crystallographic and refinement data for $BaTa_2O_6$ and $[Ba_3F]Ta_4O_{12}F$ can be found in Table 1. Atomic coordinates are listed in Table 2 and Table 3 and selected interatomic distances are provided in Table 4.

Table 2. Atomic coordinates ($\times 10^4$) and equivalent isotropic displacement parameters ($Å^2 \times 10^3$) for $BaTa_2O_6$

Atom	x	y	z	U_{eq} [$Å^2$]
Ta(1)	0	6470.0(3)	0	14.42(13)
O(1)	0	6260(20)	-5000	8(4)
O(2)	-1356(5)	4322(2)	0	17.5(10)
O(3)	-1563(3)	6873(6)	0	30.5(15)
O(4)	-303(10)	6390(8)	-5000	7(2)
Ba(1)	-3333.33	3333.33	5000	27.0(2)
Ba(2)	0	10000	5000	37.7(3)

Table 3. Atomic coordinates ($\times 10^4$) and equivalent isotropic displacement parameters ($Å^2 \times 10^3$) for $[Ba_3F]Ta_4O_{12}F$

Atom	x	y	z	U_{eq} [$Å^2$]
Ta(1)	5439(2)	2452.2(2)	5000	13.1(9)
Ta(2)	7931.7(2)	2068.3(2)	7499.2(3)	5.67(8)
Ba(1)	5000	5000	2470.9(6)	9.81(11)
Ba(2)	5244.1(3)	1944.9(3)	0	12.31(10)
F(1)	5975(3)	4025(3)	0	16.2(11)
F(2)	4881(3)	1061(3)	5000	18.6(8)
O(2)	4881(3)	1061(3)	5000	18.6(8)
O(1)	6462(2)	1983(2)	6852(4)	9.5(5)
O(3)	7611(3)	2389(3)	10000	9.5(11)
O(4)	8345(3)	1655(3)	5000	7.8(10)
O(5)	4477(2)	2922(2)	6896(4)	8.8(5)
O(6)	6095(3)	3905(3)	5000	7.3(11)

Table 4. Selected Interatomic Distances (Å) for $BaTa_2O_6$ and $[Ba_3F]Ta_4O_{12}F$

	$BaTa_2O_6$	$[Ba_3F]Ta_4O_{12}F$
Ta(1)-O(1)	1.992(3)	1.997(3)
Ta(1)-O(2)	2.007(3)	
Ta(1)-O(3)	1.9190(11)	
Ta(1)-O(4)	2.0009(14)	
Ta(1)-O(5)		1.972(3)
Ta(1)-O(6)		2.0341(19)
Ta(2)-O(1)		1.941(3)
Ta(2)-O(3)		1.9629(17)
Ta(2)-O(4)		2.017(2)
Ta(2)-O(5)		2.024(3)

The structure of $BaTa_2O_6$ consists of TaO_6 octahedra that edge-share *via* equatorial O(2) to form Ta_2O_{10} dimers (Figure 2a), Each Ta_2O_{10} dimer corner-shares *via* the axial trans O(1) to two dimers, one above and one below, to form infinite stacks of Ta_2O_{10} dimers (Figure 2b). These stacks corner-share *via* the equatorial O(3) to four other stacks to create two types of channels, hexagonal and triangular. The barium atoms are located in both types of channels (Figure 2c). The overall coordination environment of each Ta is best described as $TaO_{2/2}O_{2/2}O_{2/2}$ with Ta-O bond lengths of 1.9834(11) Å, 2.007(3) Å, 1.9190(11) Å, consistent with the expected interatomic distances for a Ta^{5+}-O bond.

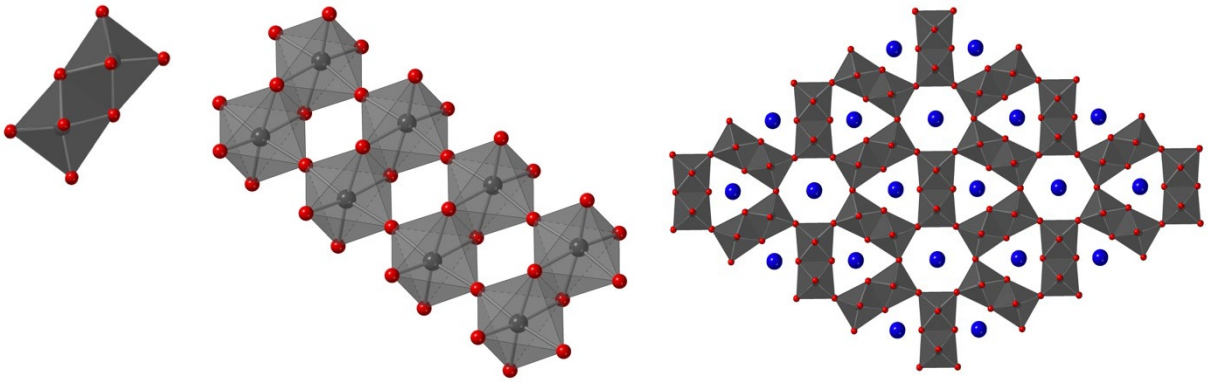

(a) (b) (c)

Figure 2. Representation of (a) Ta_2O_{10} dimers, (b) stacks of Ta_2O_{10} dimers, and (c) crystal structure of $BaTa_2O_6$. Ta in grey polyhedra, Ba in blue, and O in red.

The morphology of this structure is distinctly different from the previously reported three polymorphs shown in Figure 3. The orthorhombic polymorph $BaTa_2O_6$-O is most closely related in that it also consists of corner-sharing stacks of Ta_2O_{10} dimers. However, in the case of the orthorhombic polymorph, the Ta_2O_{10} dimer stacks have a different connectivity to other stacks; furthermore, the TaO_6 octahedra are substantially more distorted than in the new hexagonal phase. The hexagonal bronze polymorph $BaTa_2O_6$-H also contains the stacks of Ta_2O_{10} dimers, however they are connected to both stacks of Ta_2O_{10} dimers and stacks of TaO_6 octahedra. The tetragonal phase consists of all corner-sharing TaO_6 octahedra. It is worth noting that this new hexagonal polymorph was synthesized at 800 °C, substantially lower than the other hexagonal polymorph obtained by Mumme[1], which was synthesized at 1400 °C.

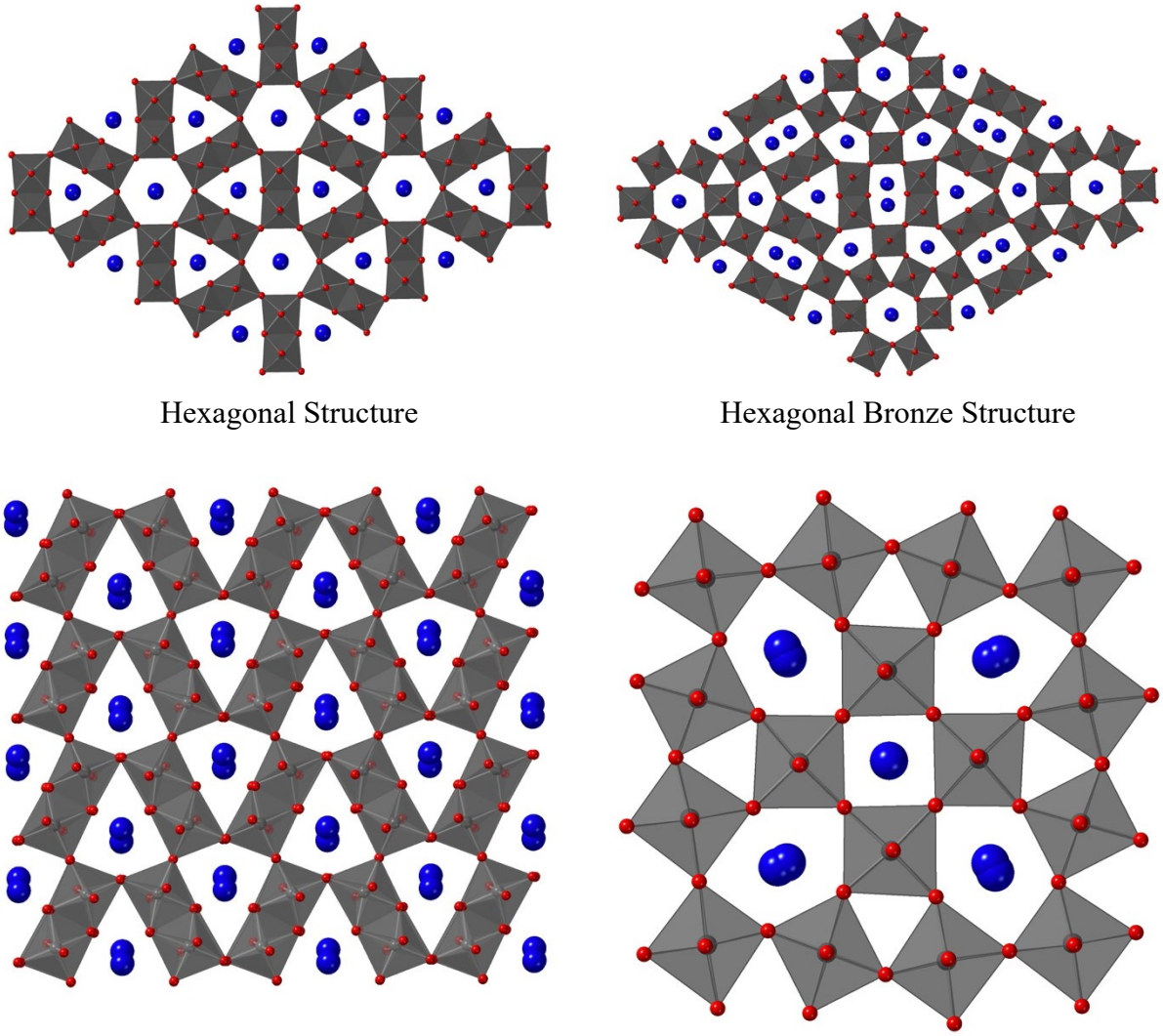

Figure 3. Crystal structures of the different polymorphs of $BaTa_2O_6$. Ta in grey polyhedra, Ba in blue, and O in red.

Performing the same synthesis except using a rubidium rather than a cesium based chloride fluoride flux resulted in the salt inclusion phase, $[Ba_3F]Ta_4O_{12}F$ (Fig. 4a). The structure consists of slightly zig-zagging chains of trans corner-sharing (*via* O(3) and O(4)), TaO_6 octahedra that corner-share their equatorial O(1) and O(5) oxygens with TaO_5F octahedra. Each TaO_5F octahedra connects to two adjacent TaO_6 chain octahedra, creating the zig-zag shape. The TaO_5F octahedra are connected to each other *via* corner-sharing through O(6). The F(2) atom on the TaO_5F octahedra is connected to Ba(2) (Fig. 4b).

Ba(1) and F(1) form the core of the salt inclusion. The F(1) atoms is tetrahedrally coordinated to four Ba(1) in the Ba_6F_2 salt inclusion groups (Fig. 4c-d). The two central bariums, Ba(1), are only bonded to the F(1) of the salt inclusion, as well as *via* long bonds to O(5) and O(6), while Ba(2) is bonded to F(1) of the salt inclusion as well as to F(2) that is part of the TaO_5F octahedra.

Tantalum oxyfluoride units, such as $TaOF_5$, TaO_2F_5, are well known in tantalum oxyfluoride chemistry [34–39] and are created in fluorine rich environments, such as aqueous HF or fluoride containing high temperature solutions. It is interesting that in the case of CsCl/CsF (m.p. 440 °C) the $BaTa_2O_6$ phase crystallized and in RbCl/RbF (m.p. 560 °C) the SIM $[Ba_3F]Ta_4O_{12}F$. The eutectic melting points of the fluxes are over 100 degrees apart and it is possible that this changes the kinetics of the initial phase that crystallizes, suggesting that at least one, if not both of the two phases is a kinetic product. To explore the stability of $BaTa_2O_6$ relative to the other known polymorphs, we performed DFT calculations.

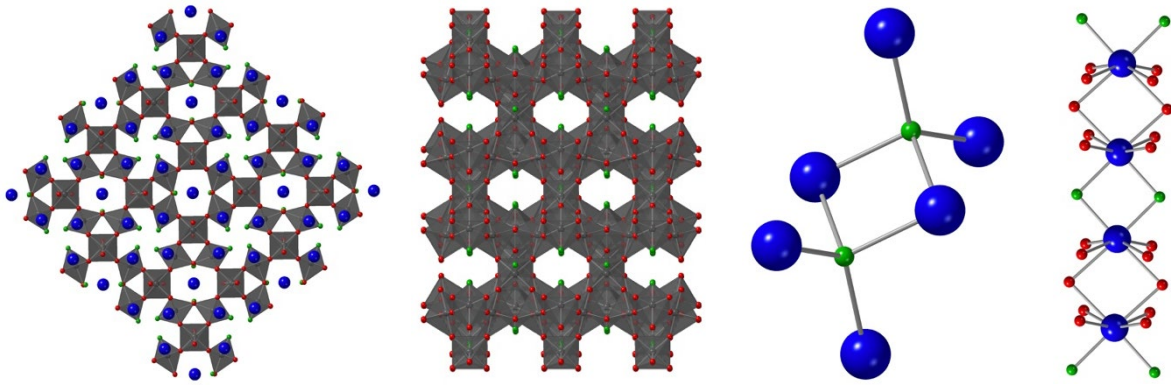

Figure 4. a) Crystal structure of $[Ba_3F]Ta_4O_{12}F$. b) Framework of $[Ba_3F]Ta_4O_{12}F$ – salt inclusion and barium atoms not shown. c) Ba_6F_2 salt inclusion. d) extended salt inclusion. Ta in grey polyhedra, Ba in blue, F in green and O in red.

To evaluate the stability of the four polymorphs, we conducted DFT studies to obtain their enthalpies of formation using OQMD as a reference for the energies for the elements. The calculations show that the most enthalpically favorable $BaTa_2O_6$ polymorphic modification is the orthorhombic one, with a $\Delta_f H_{0\,K}$ of -2874.29 kJ/mol. The tetragonal and hexagonal bronze phases are only 6.08 and 16.53 kJ/mol higher in energy (2868.21 and 2857.75 kJ/mol,

respectively), which indicates that these two phases can compete with the most stable orthorhombic phase. This result is in a good agreement with experimental evidence of simultaneous formation of all three phases in one flux reaction [10]. Given that the hexagonal polymorph forms more readily at higher temperatures (above 1300 °C), whereas the enthalpically favorable orthorhombic polymorph already forms at lower temperatures, one can surmise that the entropic factor starts playing a more important role as the reaction temperature increases, out-competing the 16.53 kJ/mol enthalpy energy difference between the polymorphs at higher temperatures. Interestingly, the new hexagonal polymorph with a $\Delta_f H_{0\,K}$ of -2825.11 kJ/mol has a 49.17 kJ/mol higher energy than the orthorhombic phase. Despite a large energy difference, $BaTa_2O_6$-H-new forms at relatively low temperatures, below 800 °C, and therefore can be considered to be a kinetically trapped product.

Conclusion

It is well-documented that using a flux can favor the formation of a kinetically stable product due to lower reaction temperatures. In this work we identified a new polymorph of $BaTa_2O_6$ as well as a new salt-inclusion material $[Ba_3F]Ta_4O_{12}F$. $BaTa_2O_6$ crystallizes as a hexagonal structure with *P*6/*mmm* symmetry from a CsCl/CsF flux and contains the same structural units that have been observed in the other three polymorphs. DFT calculations revealed that the new $BaTa_2O_6$ structure is the least enthalpically favorable polymorph, which likely is stabilized by kinetic factors. The salt inclusion material $[Ba_3F]Ta_4O_{12}F$ crystallizes in the tetragonal space group $P4_2/mnm$ and consists of a $Ta_4O_{12}F^{5-}$ framework with tetrahedral Ba_4F salt inclusions in it.

Acknowledgements

Financial support for this work was provided by the National Science Foundation under award DMR-1806279 and is gratefully acknowledged.

Supporting Information

EDS for $BaTa_2O_6$. CSD 2026551 and 2026552 contain the supplementary crystallographic data for this paper. The data can be obtained free of charge from The Cambridge Crystallographic Data Centre *via* www.ccdc.cam.ac.uk/structures.

References

[1] W.G. Mumme, I.E. Grey, R.S. Roth, T.A. Vanderah, J. Solid State Chem. 180 (2007) 2429–2436. https://doi.org/10.1016/j.jssc.2007.06.014.

[2] G. Layden, Mater. Res. Bull. 3 (1968) 349–360.

[3] W. Zhang, N. Kumada, T. Takei, J. Yamanaka, N. Kinomura, Mater. Res. Bull. 40 (2005) 1177–1186. https://doi.org/10.1016/j.materresbull.2005.03.028.

[4] M. Ilhan, Solid State Sci. 38 (2014) 160–168. https://doi.org/10.1016/j.solidstatesciences.2014.08.015.

[5] L.H. Brixner, J. Am. Chem. Soc. 80 (1958) 3214–3215. https://doi.org/10.1021/ja01546a011.

[6] C.D. Ling, M. Avdeev, V. V. Kharton, A.A. Yaremchenko, R.B. Macquart, M. Hoelzel, Chem. Mater. 22 (2010) 532–540. https://doi.org/10.1021/cm903170t.

[7] J. Shannon, L. Katz, Acta Crystallogr. B. 26 (1970) 102.

[8] F. Galasso, L. Katz, Acta Crystallogr. 14 (1961) 647–650. https://doi.org/10.1107/s0365110x61001972.

[9] L.M. Kovba, L.N. Lykova, M. V. Paromova, L.M. Lopato, A. V. Shevchenko, Russ. J. Inorg. Chem. 20 (1977) 2845−2847.

[10] G. Layden, Mater. Res. Bull. 2 (1967) 533–539.

[11] F. Galasso, L. Katz, R. Ward, J. Am. Chem. Soc. 81 (1959) 5898–5899. https://doi.org/10.1021/ja01531a013.

[12] F. Galasso, G. Layden, G. Ganung, Mat. Res. Bull. 3 (1968) 397–407.

[13] I.G. Ismailzade, Sov. Physics, Cryst. (1960) 618.

[14] I.G. Ismailzade, Dokl. Adad. Nauk Azerbyzhan SSSR. (1959).

[15] N.G. Kim, M. Avdeev, Y. Il Kim, J. Alloys Compd. 815 (2020) 152420. https://doi.org/10.1016/j.jallcom.2019.152420.

[16] O. Savborg, M. Lundberg, J. Solid State Chem. 57 (1985) 135–142.

[17] D.E. Bugaris, H.C. Zur Loye, Angew. Chemie - Int. Ed. 51 (2012) 3780–3811. https://doi.org/10.1002/anie.201102676.

[18] C.A. Juillerat, V. V. Klepov, G. Morrison, K.A. Pace, H.C. Zur Loye, Dalt. Trans. 48 (2019) 3162–3181. https://doi.org/10.1039/c8dt04675a.

[19] G. Morrison, M.D. Smith, H.C. Zur Loye, J. Am. Chem. Soc. 138 (2016) 7121–7129. https://doi.org/10.1021/jacs.6b03205.

[20] C.A. Juillerat, E.E. Moore, G. Morrison, M.D. Smith, T. Besmann, H.C. Zur Loye, Inorg. Chem. 57 (2018) 11606–11615. https://doi.org/10.1021/acs.inorgchem.8b01729.

[21] V. V. Klepov, C.A. Juillerat, E. V. Alekseev, H.C. Zur Loye, Inorg. Chem. 58 (2019) 724–736. https://doi.org/10.1021/acs.inorgchem.8b02906.

[22] APEX3, APEX3, version 2016.5-0; SAINT+, version 8.37A; Bruker AXS, Inc., Madison, Wisconsin, USA, (2016).

[23] L. Krause, R. Herbst-Irmer, G.M. Sheldrick, D. Stalke, J. Appl. Crystallogr. 48 (2015) 3–10. https://doi.org/10.1107/S1600576714022985.

[24] O. V. Dolomanov, L.J. Bourhis, R.J. Gildea, J.A.K. Howard, H. Puschmann, OLEX2: A complete structure solution, refinement and analysis program, J. Appl. Crystallogr. 42 (2009) 339–341. https://doi.org/10.1107/S0021889808042726.

[25] G.M. Sheldrick, Crystal structure refinement with SHELXL, Acta Crystallogr. Sect. C Struct. Chem. 71 (2015) 3–8. https://doi.org/10.1107/S2053229614024218.

[26] G. Kresse, J. Furthmüller, Comput. Mater. Sci. 6 (1996) 15–50. https://doi.org/10.1016/0927-0256(96)00008-0.

[27] G. Kresse, J. Furthmüller, Phys. Rev. B - Condens. Matter Mater. Phys. 54 (1996) 11169–11186. https://doi.org/10.1103/PhysRevB.54.11169.

[28] J.P. Perdew, K. Burke, M. Ernzerhof, Phys. Rev. Lett. 77 (1996) 3865–3868. https://doi.org/10.1103/PhysRevLett.77.3865.

[29] P.E. Bloechl, Phys. Rev. B. 50 (1994) 17953–17979.

[30] G. Kresse, D. Joubert, Phys. Rev. B - Condens. Matter Mater. Phys. 59 (1999) 1758–1775. https://doi.org/10.1103/PhysRevB.59.1758.

[31] S. Kirklin, J.E. Saal, B. Meredig, A. Thompson, J.W. Doak, M. Aykol, S. Rühl, C. Wolverton, Npj Comput. Mater. 1 (2015). https://doi.org/10.1038/npjcompumats.2015.10.

[32] C.A. Juillerat, V. Kocevski, G. Morrison, S.G. Karakalos, D. Patil, S.T. Misture, T.M. Besmann, H.C. Zur Loye, Inorg. Chem. Front. 6 (2019) 3203–3214. https://doi.org/10.1039/c9qi00537d.

[33] A.M. Latshaw, B.O. Wilkins, K.D. Hughey, J. Yeon, D.E. Williams, T.T. Tran, P.S. Halasyamani, H.C. Zur Loye, CrystEngComm. 17 (2015) 4654–4661.

https://doi.org/10.1039/c5ce00671f.

[34] M. Vlasse, J.P. Chaminade, M. Pouchard, Mat. Res. Bull. 8 (1973) 117–126.

[35] M. Vlasse, J.P. Chaminade, J.C. Massies, M. Pouchard, J. Solid State Chem. 12 (1974) 102–109.

[36] M. Vlasse, J.P. Boukhari, J.P. Chaminade, M. Pouchard, Mat. Res. Bull. 14 (1979) 101–108.

[37] G. Pourroy, P. Poix, J.P. Sanchez, J. Solid State Chem. 74 (1988) 27–33.

[38] G. Blasse, D. G.J., Solid State Commun. 90 (1994) 595–597.

[39] J. Zhao, X. Wang, N. Li, R. Xu, J. Liu, Y. Li, Electrochem. Commun. 10 (2008) 273–276. https://doi.org/10.1016/j.elecom.2007.12.005.